Electrochimica Acta 514 (2025) 145643

Contents lists available at ScienceDirect

Electrochimica Acta

journal homepage: www.journals.elsevier.com/electrochimica-acta

New electrochemical approach for assessing surface tension and its role in atmospheric particle growth

Kristijan Vidović [a,b,*], Samo B. Hočevar [a,*], Kumar Sarang [a], Ivan Konjević [a], Nikola Tasić [a], Irena Ciglenečki [b]

[a] Department of Analytical Chemistry, National Institute of Chemistry, Hajdrihova 19, Ljubljana 1000, Slovenia
[b] Ruđer Bošković Institute, Division for Marine and Environmental Research, Laboratory for Physical Oceanography and Chemistry of Aquatic Systems, Bijenička cesta 54, Zagreb 10000, Croatia

ARTICLE INFO

Keywords:
Surface-active substances
Surface tension
Non-faradaic electrochemistry
Electrochemical impedance spectroscopy
New particle formation

ABSTRACT

Despite numerous studies addressing the complex role of surface-active substances (SAS) in cloud condensation nuclei, a significant gap exists in understanding their intrinsic importance and involvement, particularly in gas uptake and atmospheric particle growth. In this study, we advance the application of electrochemistry in this field and provide new insights into the role and impact of hydrophilic/hydrophobic SAS on the growth of atmospheric aerosol particles. We employed an innovative approach based on non-faradaic electrochemistry. A change of the measured capacitive current ($dI_{capacity}$) is caused by the adsorption of SAS on the electrode surface, which is directly proportional to the change of surface tension ($d\gamma$). The application of this new methodology, combined initially with the mercury electrode, demonstrated significantly higher sensitivity and reliability compared to other conventional tensiometric methods for measuring surface tension. Moreover, the effectiveness of this strategy was tested and validated using the environmentally friendly bismuth electrode as an excellent alternative.

1. Introduction

Surface-active substances (SAS) are organic compounds that frequently occur in atmospheric aerosol particles, settle on their boundary surface as a film, and have far-reaching effects on climate and health [1,2]. The SAS directly modify aerosol particles' optical properties by changing their morphology, impacting their ability to scatter or absorb solar radiation [3]. SAS influence climate indirectly by aiding particle activation, providing cloud condensation nuclei (CCN), thus affecting cloud formation [4,5]. Through adsorption onto particle surfaces, SAS reduce their surface tension (γ), which, in line with Köhler's theory, is a primary factor governing critical droplet diameter and supersaturation *via* the Kelvin effect [2,6].

It was demonstrated that the presence of SAS in atmospheric particles can stabilize and extend the particles' lifetime [7]. However, their impact on the new particle formation (NPF) remains relatively under-explored. Our recent study [8] revealed a clear relationship between nucleation mode particles' condensation growth rate and their surface activity in the coastal environment, particularly in the presence of smaller carboxylic acids such as formic, acetic, lactic, and maleic acids. Despite their significance, no existing technique could accurately determine the change in the surface tension caused by SAS in the particles at atmospherically relevant very low concentrations. The surface tension (γ) of bulk aqueous samples can be effectively studied using various dynamic and static methods, including the Wilhelm plate, de Nouy tensiometer, oscillating bubble tensiometer, axisymmetric pendant drop tensiometer, and ring-down tensiometer [1,9–12]. A drawback of these methods is their sensitivity to the salt content, which increases γ in an aqueous solution and is inevitable when studying atmospheric particles [1,13]. In such mixtures, at higher salt concentrations, the solubility of organic compounds may decrease, referred to as "salting out" [13]. This can enhance the formation of organic film at the gas-solution interface, resulting in γ decrease, and potentially counteract the increase caused by the inorganic salts, leading to the over or under-estimation of the SAS [1,14].

To address this gap, we propose revisiting an often-overlooked electrochemical technique known as polarographic "tensammetry" [15]. In the past, electrochemical tensiometry, in conjunction with a

* Corresponding authors.
E-mail addresses: kristijan.vidovic@ki.si (K. Vidović), samo.hocevar@ki.si (S.B. Hočevar).

https://doi.org/10.1016/j.electacta.2025.145643
Received 13 November 2024; Received in revised form 11 December 2024; Accepted 2 January 2025
Available online 3 January 2025

mercury electrode, was employed to study the adsorption of various organic molecules [16–19]. As the electrode-electrolyte interface simulates an electrical capacitor, the adsorption of SAS onto the mercury electrode induces a decrease in the capacity, which can be measured as an attenuation of the capacitive current ($I_{capacity}$) [20–24]. The adsorption of SAS reduces the mercury electrode's γ [25], thus, by measuring the $dI_{capacity}$ one can obtain valuable insights into the γ alteration caused by specific SAS [26,27]. Recently, Alison Bain 2024 [28] highlighted the strong need to develop new methods and techniques to better understand surface tension of aerosol particles. Within the reviewed work, the author concludes no single existing technique (pendant drop, atomic force microscopy, oscillating droplet, droplet coalescence & elastic backscattering, stroboscopic imaging, high-framerate imaging of droplets impacting surfaces, rainbow refractometry, quasielastic light scattering from spontaneous capillary-wave resonances, electric-field induced shape oscillations, and droplet deformation) can be used to investigate all possible systems of interest in aerosol science. Accurately presenting the aerosol or atmospheric particle surface tension potentially increases the accuracy in predicting CCN formation, concentrations, hygroscopic growth, and the morphology of spray-dried particles.

The present study introduces a new interpretation of the electrochemical methodology for the first time, particularly regarding the quantification of γ decrease caused by SAS in atmospheric aerosol particles. Additionally, we demonstrate an advancement of electrochemical tensiometry by using an environmentally friendly bismuth electrode as an alternative to its mercury counterpart. The implementation of the new methodology shows its markedly enhanced sensitivity compared to conventional tensiometric methods, highlighting its pivotal role in understanding atmospheric particle growth processes and the impact of SAS in atmospheric research.

2. Experimental

2.1. Determination of γ decrease using the electrochemical approach

The electrocapillary Eq. (1) portrays the correlation between γ and electrode potential (E) and depicts the relationship between various electrochemical variables [27,29–31]. Thus, it is possible to indirectly acquire information about γ by measuring other relevant electrochemical parameters, as follows:

$$-d\gamma = \sigma^M dE + \Gamma_{Na^+(H_2O)} d\mu_{NaCl} + \Gamma_{M(H_2O)} d\mu_M \quad (1)$$

where $d\gamma$ is the change of surface tension, σ^M is the surface charge on the electrode, and terms Γ and μ correspond to the surface excess concentration and chemical potential of the electrolyte and organic molecules, respectively. dE is the applied potential to the working electrode. Eq. (1) involves experimentally significant quantities, either controllable or measurable. From the electrocapillary equation, it is evident that σ^M can be expressed as: [27,30,32]

$$\sigma^M = -\left(\frac{\partial \gamma}{\partial E}\right)_{\mu_{NaCl},\mu_M} \quad (2)$$

According to Eq. (2), the electrode's amount of σ^M directly correlates with $d\gamma$ and is an electrochemically measurable parameter. The amount of σ^M can be measured directly or indirectly by measuring the $I_{capacity}$ or capacity of the electrochemical system [33]. The $I_{capacity}$ can be expressed as the number of charges per unit of time as Eq. (3), [27] while the double-layer capacitance (C_{dl}) of the electrochemical system as Eq. (4): [27,30,34,35]

$$I_{capacity} = \frac{d\sigma^M}{dt} \quad (3)$$

$$C_{dl} = \left(\frac{\partial \sigma^M}{\partial E}\right) \quad (4)$$

Therefore, by measuring either $I_{capacity}$ or C_{dl} in the blank electrolyte solution of a specific electrochemical system (such as a static mercury drop electrode (SMDE) – in 0.55 M NaCl or a bismuth electrode in 0.1 M $NaClO_4$) and comparing it to that of the same system in the presence of SAS, one can attain insights into the $d\gamma$ induced by these SAS [25,36] (Eq. (1)).

SAS adsorption onto the SMDE is the most favored within a narrow potential range [16]. SAS influence the electrode/electrolyte interface by adsorbing onto the electrode surface, which is analogous to an electrical capacitor [16,17,36,37]. The adsorbed SAS act as dielectrics [26] and compete with water molecules for available sites on the electrode surface [36]. SAS generally interact less with charges than water, which favors their adsorption on less charged electrodes [22]. If the σ^M is too positive or negative, the $dI_{capacity}$ due to the presence of SAS is barely recognizable [25]. When adsorbed onto the electrode, these dielectrics (SAS) reduce the interface's capacitance by diminishing the double-layer capacitor's active surface area and decreasing its permittivity [20,33,38]. By reducing the interface's capacitance and subsequently diminishing the quantity of σ^M, the adsorbed molecules consequently lower the γ. Since γ is directly linked to the C_{dl}, the electrocapillary curve can be constructed based on the C_{dl} using Eq. (5): [27, 33]

$$\gamma = \int_{E_{p.z.c.}}^{E} \int C_{dl} dE \quad (5)$$

For such operations, knowing the potential of zero charge (p.z.c.) is essential. Each electrode within a defined electrochemical system reaches a state where the surface charge approaches zero, known as the p.z.c. [27,35] This specific point (potential) can be experimentally determined for individual electrochemical systems [35,39–41]. At the p.z.c., the γ of the electrode is the highest (SI Figure S1). Consequently, any decrease in the $I_{capacity}$ or C_{dl} (directly related to γ) can be attributed solely to SAS. The ionic strength of the electrolyte is held constant, eliminating its influence as a confounding factor. This allows for a more isolated and accurate assessment of the impact of SAS on the γ.

2.2. Alternative current (AC) voltammetry measurements at the SMDE

AC voltammetric measurements were conducted using a Metrohm PGSTAT 128 N with a multi-mode mercury electrode (MME) equipped with a 663 VA stand and IME interface. The MME was operated in a SMDE mode (with an electrode diameter of 0.2 mm) as the working electrode. The reference electrode was Ag|AgCl (3 M KCl) in all experiments, and a graphite electrode served as the counter electrode. The experiments were conducted in a 10 mL glass electrochemical cell containing a standard electrolyte of 0.55 M NaCl. The process involved accumulation and stirring at the initial potential of −0.6 V. The AC voltage had an amplitude of 10 mV and the frequency was 77.35 Hz. Optimization of frequency and AC amplitude resulted in a phase angle close to 90°, enabling efficient extraction of the system's $I_{capacity}$.

2.3. Electrochemical impedance spectroscopy (EIS) measurements at the bismuth bulk electrode (BiBE)

EIS measurements were performed using a PalmSens4 with a frequency response analyzer (FRA) module. A homemade BiBE (disc, $r = 2$ mm) served as the working electrode, with an Ag|AgCl (3 M KCl) and a platinum wire as the reference and counter electrode, respectively. All EIS measurements were conducted in a 10 mL glass electrochemical cell containing 0.1 M $NaClO_4$ as an electrolyte. Prior to the EIS measurement, the electrode was held at −1.0 V for 1 min to clean the BiBE surface from various oxides. Following this, the potential was switched to −0.75 V, where the SAS were accumulated by stirring for 5 min. After the accumulation, EIS measurements involved a frequency scan from 1

to 10,000 Hz at the potential of −0.75 V. The excitation AC signal had an amplitude of 4 mV.

2.4. Single-frequency EIS measurement for determination of the p.z.c. at BiBE

Single-frequency EIS was employed to investigate the differential capacitance (C_{diff}) as a function of applied electrode potential [35, 40–42] for BiBE in 0.1 M $NaClO_4$. In the absence of specific adsorption (in the blank electrolyte of 0.1 M $NaClO_4$), the minimum in the C_{diff} vs. E curve corresponds to the p.z.c. (Figure S8B). The single-frequency EIS experiment was conducted with an amplitude of 4 mV at a frequency of 20 Hz, over the potential range of −0.4 V to −1.6 V. The C_{diff} was determined from the imaginary part of impedance as follows: [35]

$$C_{diff} = -(\omega Z_{Im})^{-1} \quad (6)$$

where ω denotes the angular frequency, and Z_{Im} denotes the imaginary part of the impedance.

2.5. Sampling site

Size-segregated atmospheric particle samples, including particulate matter with a diameter of 1 micrometer or less (PM_1), as well as particle number size distributions (PNSD), were simultaneously collected at an urban background site in Ljubljana, Slovenia (population approximately 300,000). Ljubljana spans 163.8 km^2 and is situated in the Ljubljana basin in Central Slovenia, nestled between the Alps and the Karst. It is positioned 410 km south of Munich 720 km east of Zurich, 250 km east of Venice, 380 km southwest of Vienna, 124 km west of Zagreb, and 480 km southwest of Budapest. Its climate is oceanic, bordering on a humid subtropical climate, featuring continental traits such as warm summers and moderately cold winters. Precipitation is relatively evenly distributed throughout the seasons, although winter and spring are drier than summer and autumn. Details of the method for online particle sampling (PNSD) and offline particle sampling (extraction of ultrafine mode particles and PM_1), are provided within the SI method section.

2.6. Chemicals

Triton-X-100 (TX-100) >99 % (Sigma-Aldrich, Saint Louis, MO, USA) was used without further purification; Lactic acid >90 % (Fluka, New Jersey, USA). Maleic acid 99 % (Acros organics, New Jersey, USA).

The electrolytes for electrochemical measurements were prepared volumetrically using sodium chloride (NaCl, Sigma Aldrich, Denmark, ACS reagent, >99.0 %) and sodium perchlorate ($NaClO_4$, Sigma Aldrich, USA, ACS reagent, 98.0 %). For the AC voltammetry system with a mercury electrode, a base electrolyte of 0.55 M NaCl was employed, while for the EIS system with a bismuth electrode, 0.1 M $NaClO_4$ was used as the base electrolyte.

All standard solutions, including TX-100, lactic acid, and maleic acid, were prepared using water from a Milli-Q system. The stock solutions of each compound were prepared by accurately weighing approximately 20 mg of the respective standard. These stock solutions were subsequently utilized to measure the decrease in surface tension through standard additions to the electrolyte solutions. The calibration concentration range used for TX-100 was 0.015 – 1 ppm, while for lactic acid was 0.1 – 1800 ppm. For the pendant drop tensiometric measurements, calibration solutions with higher concentrations (TX-100: 32 – 500 ppm; lactic acid: 30 000 – 400 000 ppm) were prepared.

3. Results and discussion

3.1. AC voltammetry (Out-of-Phase): a new interpretation of γ measurement in extracted ultrafine mode particles at the SMDE

Fig. 1 and Figure S2 in SI show the AC voltammograms observed at the SMDE in the presence of extracted ultrafine mode atmospheric particles (dotted red line) and the AC voltammograms recorded in the 0.55 M NaCl blank electrolyte (black line). In the presence of the ultrafine mode atmospheric particle water extract, there is a decrease in the $I_{capacity}$ (at −0.6 V) with respect to the blank electrolyte. The decrease in the $I_{capacity}$ results from the adsorption of SAS on the electrode surface (for more method details, refer to SI) [20,21,24,33,43]. At the same time, the adsorption of SAS causes a decrease in the γ of the SMDE [36, 44]. The decrease in γ can be quantified by measuring the difference in $I_{capacity}$ between the base electrolyte and the solution containing SAS [25,27,36].

In the case of the SMDE and NaCl as an electrolyte, the p.z.c. is at approximately −0.6 V vs. Ag|AgCl reference electrode [18]. It is important to note that ionic strength can influence the p.z.c. [27,45]. In the case of electrochemical measurements, 0.55 M NaCl serves as a supporting electrolyte, and the salt content from the extracted particles is not expected to influence the overall ionic strength significantly. Therefore, the decrease in $I_{capacity}$ is a direct consequence of the SAS adsorption only.

Using equations 1 – 5, we derived Eq. (7) to quantify the relative $d\gamma$ (expressed in %) caused by the SAS present within the water extracts of the ultrafine mode atmospheric particles. $d\gamma$ (%) is obtained by measuring $dI_{capacity}$ relative to the blank electrolyte at the p.z.c. as follows:

$$d\gamma(\%) = \left(1 - \frac{I_{capacity}}{I_{capacity_0}}\right) \cdot 100\% \quad (7)$$

where $I_{capacity_0}$ is the capacitive current obtained in the blank electrolyte, and $I_{capacity}$ is the capacitive current obtained in the ultrafine mode atmospheric particle water extract solution at p.z.c. Table 1 presents $d\gamma$ (%) observed in the water extracts of ultrafine mode atmospheric particles collected from the urban area of Ljubljana (Slovenia).

Table 1 indicates that the water-extracted organic SAS from ultrafine mode atmospheric particles decrease the γ by approximately 15 to 19.5 %. To evaluate the quality and consistency of the electrochemically measured γ data, we employed a modified Szyszkowski-Langmuir (S-L) equation: [46]

$$1 - \frac{\gamma}{\gamma_w} = b \cdot \ln\left(1 + \frac{C}{a}\right) \quad (8)$$

The term on the left side of Eq. (8) can be easily identified as the term on the right side of Eq. (7). Here, γ represents the surface tension of the organic molecules, while γ_w represents the surface tension of water. The total term $1\text{-}\gamma/\gamma_w$ reflects the relative $d\gamma$ (%) compared to the γ_w. On the right side of Eq. (8), b represents a constant property of the homologous series of the organic compounds involved, a represents a constant property specific to each organic compound, and C represents the WSOC concentration [1,4,46].

Fig. 2A demonstrates that the measured $d\gamma$ (%) in the ultrafine mode atmospheric particle water extracts follows the S-L equation very well ($R^2 = 0.75$, $\chi^2 = 0.0005$). The curve corresponds to $1\text{-}\gamma/\gamma_w = 0.03 \cdot \ln(1 + 59.8 \cdot C)$, derived by fitting the modified S-L Eq. (8). The dγ (%) behavior with increasing concentration of WSOC has already been documented in the literature [47–49]. In addition, Fig. 2A presents an intriguing observation; the data point for March 27, 2023, shown in a rectangle, exhibits a deviation from the anticipated trend, i.e., it shows a lower $d\gamma$ (%) despite a higher WSOC concentration. The effect of SAS on the $d\gamma$ (%) depends on both the concentration and the nature of SAS [20,50]. Therefore, this data point may seem atypical but cannot be described as

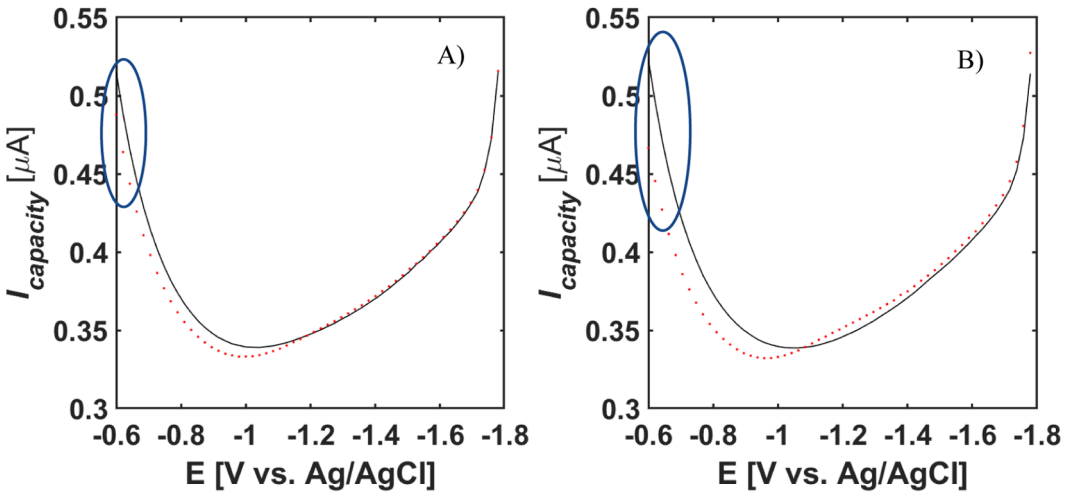

Fig. 1. AC voltammograms observed in the ultrafine mode atmospheric particle water extracts for two days: A) March 27, 2023, and B) April 1, 2023 (dotted red lines). AC voltammograms of the blank electrolyte (0.55 M NaCl, black line). The blue circle illustrates the decrease of $I_{capacity}$ at the p.z.c. (−0.6 V) in the presence of SAS compared to the blank electrolyte. See Figure S2 for voltammograms from the other observed event days.

Table 1
$I_{capacity}$ in the water extracts of ultrafine mode atmospheric particles sampled in Ljubljana and the blank electrolyte ($I_{capacity_0}$), the $d\gamma$ (%), and the concentration of water-soluble-organic carbon (WSOC) (for more method details, refer to SI).

Sample	$I_{capacity_0}$ [μA]	$I_{capacity}$ [μA]	$d\gamma$ [%]	WSOC [mg l^{-1}]
March 20, 2023	0.490	0.434	15.20	3.13
March 23, 2023	0.505	0.449	14.90	2.22
March 27, 2023	0.516	0.457	15.08	4.76
April 1, 2023	0.521	0.445	19.56	11.12
April 2, 2023	0.508	0.442	17.39	4.18
April 3, 2023	0.525	0.461	15.09	2.69
April 4, 2023	0.520	0.456	17.63	4.63

an outlier. An elevated WSOC concentration does not necessarily imply a proportional $d\gamma$ (%). Only a specific fraction of WSOC can decrease γ, depending on the nature and structural composition of the molecules involved. This particular fraction of WSOC that reduces the γ can be quantified using the normalized surface tension decrease (NSTD) parameter, representing the γ decrease normalized on the WSOC concentration, which defines the properties of those molecules [51]. Higher NSTD values indicate a more hydrophobic nature of SAS (Table 2 and SI Figure S11); hence, a reason for the deviation of the γ on March 27, 2023, from the S-L equation originates from the different nature of SAS.

To attain a deeper insight into the reliability of the electrochemical method, we measured the $d\gamma$ (%) using a single-component solution containing different concentrations of lactic acid (Fig. 2B). The empirical S-L equation has limitations in predicting the behavior of more complex mixtures [1,46]. Lactic acid was selected due to its known surface-active properties [14] and its occurrence as the dominant carboxylic acid in the analyzed samples (not shown here). Notably, the S-L equation for a single component (lactic acid) exhibits a higher degree of robustness in capturing the trend observed by the electrochemical measurements (Fig. 2B, $R^2 = 0.99$, $\chi^2 = 0.0025$) compared to the complex mixture of WSOC. In addition, validation using tensiometric measurements of the γ decrease, which were carried out with a pendant drop tensiometer (see SI methods) for different concentrations of lactic acid and TX-100, showed a significantly lower sensitivity compared to the new electrochemical methodology (SI Figure S3). The electrochemical measurements suggest that lactic acid exhibits surface-active properties even at lower concentrations, a finding that conventional tensiometric measurements cannot detect due to lower sensitivity. Such a methodology allows a better understanding of the involvement of SAS in various atmospheric processes, taking into account their dominant nature (hydrophobic/hydrophilic). To evaluate the comparability of the two methods, the relative signal decrease in surface tension at the same concentration of SAS (TX-100) was compared. The relative signal decrease was found to be consistent between the pendant drop tensiometric method (extrapolated using the S-L equation) and the electrochemical method (see SI Section 3 for details). Utilizing the derived constants (a and b) from the S-L equation (Fig. 2) and considering the γ of water of 72.8 mN m^{-1}, the absolute γ was calculated for each extracted WSOC sample obtained in Ljubljana, as illustrated in Table S1. Table S1 demonstrates that the calculated γ (59 – 62 mN m^{-1}) corresponds to typical values (52 – 72 mN m^{-1}) [1] found for short-chain carboxylic

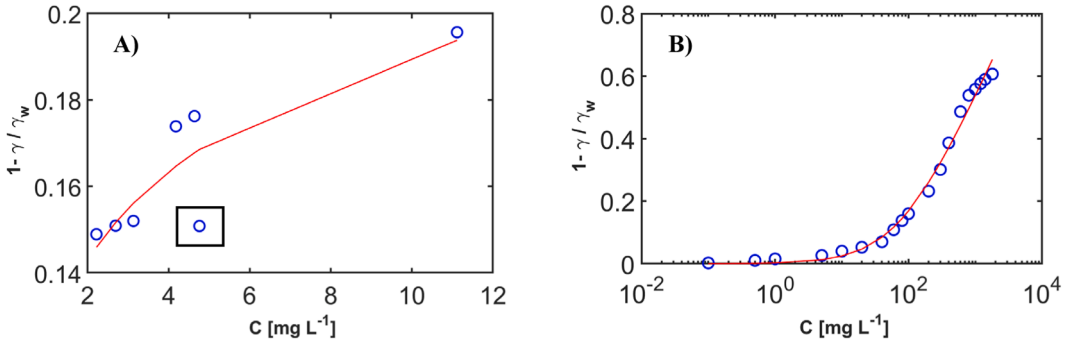

Fig. 2. A) γ decrease in the extracted ultrafine mode atmospheric particles sampled in Ljubljana with respect to water solution, plotted vs. WSOC concentrations. B) The correlation between decreased γ and lactic acid concentrations.

Table 2
J_{10}, $GR_{average}$, CS for H_2SO_4 and oxidized organic molecules (CS_{H2SO4} and CS_{OOM}), $d\gamma$ (%), and normalized surface tension decrease (NSTD) observed from the electrochemical and WSOC analysis of collected ultrafine mode particles.

	J_{10} [cm^3 s^{-1}]	$GR_{avg.}$ [nm h^{-1}]	$CS_{H_2SO_4}$ [s^{-1}]	CS_{OOM} [s^{-1}]	$d\gamma$ [%]	$d\gamma$/WSOC (NSTD)
March 23, 2023	1.26	2.01	$5.33{\cdot}10^{-3}$	$2.30{\cdot}10^{-3}$	14.90	0.067
March 27, 2023	0.52	1.85	$2.96{\cdot}10^{-3}$	$1.26{\cdot}10^{-3}$	15.08	0.032
April 1, 2023	2.07	2.89	$6.30{\cdot}10^{-3}$	$2.69{\cdot}10^{-3}$	19.56	0.018
April 2, 2023	1.49	2.65	$8.62{\cdot}10^{-3}$	$3.68{\cdot}10^{-3}$	17.39	0.042
April 3, 2023	0.40	1.70	$2.69{\cdot}10^{-3}$	$1.15{\cdot}10^{-3}$	15.09	0.056

acids (< 10 carbons) [14,52–55].

Facchini et al. [4] showed that 15 – 30 % of γ decrease is sufficient to increase the number of cloud droplets by up to 20 %. However, it has remained uncertain whether the presence of SAS and the $d\gamma$ affects the NPF, particularly the particle growth process.

3.2. EIS and BiBE: a novel environmentally friendly method for determining $d\gamma$ in extracted ultrafine mode atmospheric particles

Although mercury electrodes offer favorable properties for electrochemical measurements of γ, their application in modern electrochemistry and scientific research is severely restricted or banned due to their toxicity. S. Trasatti, in 1992 [23], demonstrated that bismuth, following mercury, exhibits the highest affinity for organic molecule adsorption on its surface within an aqueous electrolyte solution.

In this work, we obtained comparable findings from our initial study on the γ decrease of highly adsorbable TX-100 at SMDE and BiBE. In this case, the Freundlich (isotherm) adsorption constant of BiBE was marginally lower (K = 0.94) in comparison to SMDE (K = 1.18) (SI Figure S7). Driven by these discoveries, we developed an innovative approach using a BiBE.

Building upon the findings of S. Trasatti (1992) [23], our preliminary results, and knowledge of our group on bismuth electrodes [56–60], we here developed a methodology based on EIS using BiBE to determine the $d\gamma$ (%) of WSOC in ultrafine mode atmospheric particle extracts. It involves the application of, a small-amplitude AC potential across a range of frequencies to an electrochemical system and measuring the resulting impedance [61,62]. Equivalent circuit models are often used to analyze and fit the obtained experimental impedance data. These models contain circuit elements such as resistors, capacitors, and constant phase elements (CPEs) representing various electrochemical processes at the investigated interface.

The electrode material for measuring $d\gamma$ must display two essential electrochemical characteristics, i.e., a nearly ideal polarizable behavior within a specific potential range and alignment of its p.z.c. within this potential window. SI Figure S8A displays a cyclic voltammogram (CV) of the BiBE; the shape of the CV indicates that the BiBE exhibits nearly ideal polarizable behavior within the potential range of −0.5 to −1.4 V in a 0.1 M $NaClO_4$. No faradaic reactions (electron transfer reactions) are observed under these conditions; only the charging current of the electrical double layer is visible. Under such conditions, the electrode-electrolyte system can be represented as an equivalent capacitor, allowing precise measurement of its behavior in the presence of adsorbable organic molecules.

To determine the p.z.c. of BiBE, we conducted single-frequency EIS measurements [27,35,40]. SI Figure S8B illustrates the C_{diff} curve derived from single-frequency EIS measurements, plotted against the applied potentials in a 0.1 M $NaClO_4$. The minimum of the C_{diff} occurs between potentials of −0.6 V and −0.77 V. As the C_{diff} (or C_{dl}) is directly associated with σ^M and γ (see methods, Eq. (4) and 5), the minimum indicates the p.z.c. [27]. Moreover, the obtained p.z.c. (−0.75 V) of the BiBE aligns closely with values reported in the literature for various single-crystal Bi electrodes [63,64].

Such results indicate that BiBE possesses all the critical properties necessary for efficient electrochemical measurements of the $d\gamma$. The surface inhomogeneity of BiBE can be compensated by employing the CPE instead of a real capacitor within the EIS technique. The CPE is a theoretical electrical circuit element frequently utilized to represent non-ideal capacitance [65,66]. It serves as a generalization of a capacitor, particularly useful for describing systems exhibiting distributed capacitance or deviations from ideal behavior.

Fig. 3A shows a complex plane Z'', Z'-plot (a so-called Nyquist plot) of BiBE at the p.z.c. in 0.1 M $NaClO_4$ recorded by EIS. To describe the behavior of the BiBE solution interface, we employed the Frumking-Melik-Gaikazyan (FMG) equivalent circuit (inset of Fig. 3A) [66–68]. It can be seen that the FMG circuit represents the measured data very well (R^2 = 0.9992, χ^2 = 0.0002); the modified FMG equivalent circuit describes the interfacial capacitance with a CPE rather than with a real capacitor. The CPE is defined as $A^{-1}(j\omega)^{-\alpha}$, where A is a CPE coefficient representing pseudo admittance, j is a complex number notation, ω is an angular frequency, and α is a fractional exponent. When $\alpha = 1$, the CPE behaves like a real capacitor; therefore, any deviation from 1 indicates non-ideality within the electrode surface. The FMG circuit also incorporates additional elements to describe the investigated electrochemical process; R_{el} and R_{ad} represent the electrolyte and adsorption resistance, respectively, and Z_w (Warburg coefficient) accounts for semi-infinite species diffusion through the diffusion layer. Since these elements are not vital for understanding the $d\gamma$, they have been omitted from the discussion. The equivalent circuit parameters were derived by a non-linear least-square fitting of the impedance function, shown as a blue line in Fig. 3A, to the measured spectra shown by red circles. Table S2 displays the fitted parameters for each element of the equivalent circuit.

In the case of BiBE and 0.1 M $NaClO_4$, the FMG circuit was modified to achieve a more dependable regression, better reflecting the interface's physical characteristics. The FMG modification aims to enhance the accuracy of interface capacitance measurement, which is subsequently utilized to measure the $d\gamma$. Therefore, by using the modified FMG equivalent circuit, considering BiBE's affinity for adsorbable organic molecules and its ideal polarizable range within the p.z.c., the $d\gamma$ caused by organic SAS can be successfully measured using BiBE in combination with the new EIS methodology.

Table S2 shows that the deviation of BiBE from an ideal electrode (α = 1) is very low, i.e., 0.934. Values of α slightly lower than unity can be explained by somewhat lower geometric and energetic homogeneity and very weak adsorption of ions at the BiBE surface [68]. Although BiBE does not have an ideal homogeneous surface as the SMDE, the use of EIS, in combination with the modified FMG circuit containing CPE at the p.z.c., allows for reliable extraction of information on the C_{dl}, which proves to be very sensitive to the adsorption of SAS. However, the CPE often enhances the fitting quality and addresses surface inhomogeneity issues, while the pseudo admittance of CPE (parameter A) and α lack clear physical interpretations [69]. The mathematical significance of A and α is recognized in the literature [69–72], and is employed here to extract the effective double-layer capacitance (C_{eff}), using Eq. (9):

$$C_{eff} = A^{\frac{1}{\alpha}} \cdot \left[\frac{1}{R_{el}} + \frac{1}{R_{ad}}\right]^{\frac{\alpha-1}{\alpha}} \quad (9)$$

The modified FMG equivalent circuit and the developed EIS method with BiBE were further used to evaluate alterations in the C_{eff} due to the presence of extracted SAS from ultrafine mode atmospheric particles (Fig. 3B). These changes are assessed relative to the C_{eff} in the blank electrolyte.

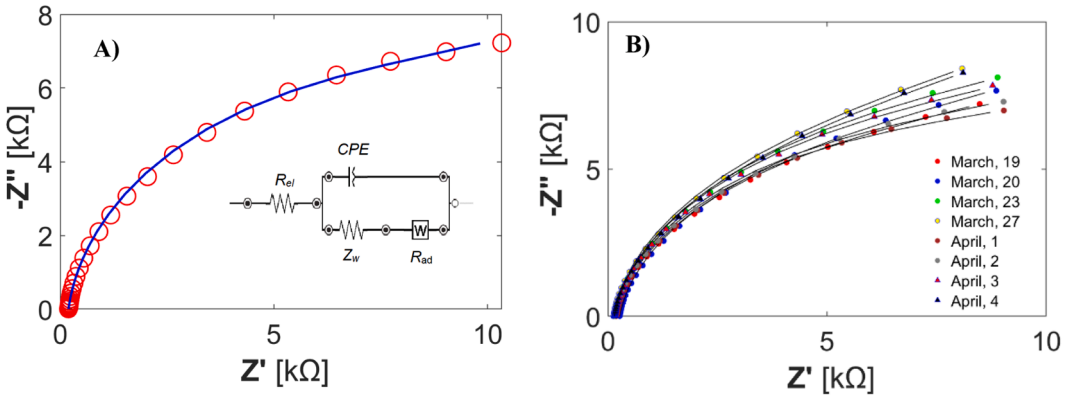

Fig. 3. Nyquist plot for BiBE in: A) 0.1 M $NaClO_4$ at −0.75 V, and B) 0.1 M $NaClO_4$ and in the presence of water extracts of ultrafine mode atmospheric particles at −0.75 V. The circles are the measured impedance data, and the line shows the fit obtained from the modified FMG circuit.

3.3. Comparison of the γ measurement: SMDE vs. BiBE

Fig. 3B demonstrates that the modified FMG equivalent circuit effectively characterizes the double-layer behavior in the presence of extracted SAS from atmospheric particles. Additionally, by applying the expression from Eq. (9), we successfully determined the C_{eff} of the CPE from the FMG equivalent circuit. The alteration in C_{eff}, observed in the presence of SAS extracted from ultrafine mode atmospheric particles, compared to C_{eff} of the blank electrolyte, is further utilized to calculate the decrease of γ.

To validate and demonstrate the reliable measurement of the γ decrease caused by SAS at BiBE using EIS, we performed several consecutive measurements of different samples using both methods, i.e., AC voltammetry at the SMDE and EIS at the BiBE. The primary distinction between AC voltammetry with SMDE and EIS with BiBE lies in the measured signal; AC voltammetry records the $I_{capacity}$, whereas EIS measures the C_{eff}. For this purpose, PM_1 samples were collected and extracted from the urban area of Ljubljana; from each extracted PM_1 sample, two aliquots were prepared for measurement using both methods. Figure S9 shows a very good agreement between measurements made by the two different methods. This suggests that BiBE can be confidently employed alongside the new EIS methodology to measure the decrease of γ induced by various SAS.

3.4. Atmospheric implication

Only a few studies report the use of electrochemistry in atmospheric research [73,74]. Using either AC voltammetry with SMDE or BiBE with EIS, it has been shown that the properties of the electrochemical double layer may be used to determine the γ decrease caused by SAS present in atmospheric aerosol particles. Atmospheric particles collected using a Berner impactor and PM sampler (PM_1) in the urban area of Ljubljana were extracted and analyzed using the new electrochemical methodology. The findings indicated that the electrochemical method enables the determination of γ decrease even in size-segregated particles (30-160 nm). The decrease in γ obtained through the electrochemical methodology aligns well with predictions made by the semi-empirical S-L equation, affirming the reliability of the proposed approach. Compared to pendant drop tensiometry, where γ is influenced by factors such as droplet size, equilibrium time, and salt effects, the electrochemical methodology relies solely on the concentration and nature of the SAS. To demonstrate further the value of this proposed electrochemical methodology, Fig. 4 and SI Figure S10 display the PNSD contour plots for seven days observed in Ljubljana. We identified various events using these contour plots and a classification scheme adapted from the literature [75–77]. Five out of seven events (shown as red circles in Fig. 4 and SI Figure S10) exhibit characteristics typical of NPF, wherein the nucleation mode particle number concentration (> 4 nm) increases and shows signs of growth. Among the five NPF events (Fig. 4 and Figure S10), two appeared in the morning (Fig. 4A and S10A), two occurred at noon (Fig. 4B and S10B), and one appeared in the evening hours (Figure S10C). In addition, pollution-related events and tailed events were observed (Figures S10D and S10E, respectively). The atmospheric particles were sampled in parallel online using SMPS and offline with a Berner impactor each day. The first three fractions sampled offline were extracted in water and further analyzed using the proposed electrochemical technique (Table 2). Notably, the decrease in γ was more significant during the noon NPF event than during the morning and evening NPF events. This suggests that a higher concentration or different nature of SAS was present on the particles during noon NPF events, possibly indicating their secondary origin through photochemical production. Table 2 also illustrates a remarkable correlation: higher $d\gamma$ corresponds to increased values of the condensation sink (CS) ($R^2 = 0.41$), higher apparent formation rate (J_{10}) ($R^2 = 0.74$), and higher average growth rate ($GR_{average}$) ($R^2 = 0.89$). See the SI method section for the calculation details of CS, apparent particle

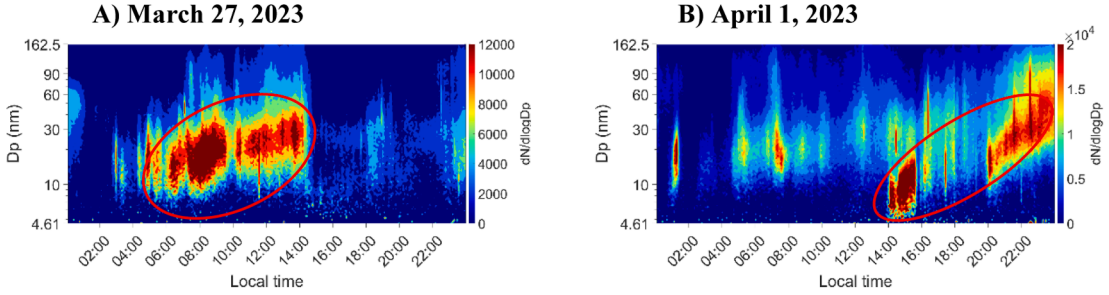

Fig. 4. Contour plots of PNSD observed in Ljubljana for: A) NPF event on March 27, 2023, and B) NPF event on April 1, 2023. The red circles indicate the occurrence of NPF events exhibiting particle growth. See Figure S10 for other observed event days.

formation rate, and growth rate. To calculate the *CS*, we considered two distinct vapors, i.e., H_2SO_4 and model oxidized organic molecules (OOM), representing the average oxidized organic molecule in the atmosphere [78]. The selection of H_2SO_4 and OOM is grounded in their significance as key vapors for particle formation and growth [78]. The rise in *CS*, alongside the decrease in γ, suggests that SAS influences vapor loss by enhancing gas-to-particle transport. Moreover, this effect is further mirrored in the increased GR_{average}. The SAS adsorbed onto the particle surface alter the interface's characteristics, enhancing the accumulation of hydrophobic or incompletely oxidized vapors at the particle surface, thus promoting heterogeneous chemistry that can contribute to particle growth [1,79].

The influence of SAS on particle growth rate depends on their structure and type [80]. Long-chain SAS, which are more hydrophobic, can form a dense, incompressible film due to attractive forces between hydrophobic tails. This film can act as a barrier for gas-to-particle mass transport. In contrast, short-chain SAS, which are less hydrophobic, form less tightly packed and more compressible films that exhibit a lower barrier to gas-to-particle transport. Therefore, short-chain SAS, such as carboxylic acids, can promote the transport of gases to the particle-gas interface, resulting in higher particle growth rates [1,2].

To assess the nature of SAS present in ultrafine mode atmospheric particles, we compared the normalized surface tension decrease (NSTD) regarding the content of WSOC vs. NSTD for known hydrophilic and hydrophobic compounds. For example, when selecting TX-100 as a hydrophobic compound (log P = 7.39, $d\gamma$/WSOC (NSTD) = 2.54) and maleic and lactic acid as hydrophilic compounds (log P = −0.3 and −0.7, $d\gamma$/WSOC (NSTD) = 0.004 and 0.005, respectively), it becomes evident (Table 2) that the NSTD observed in the water extract of ultrafine mode atmospheric particles sampled in Ljubljana aligns more closely with the hydrophilic compounds (SI Figure S11). Importantly, this methodology provides information about the nature of SAS in atmospheric particles compared to selected surrogate compounds. This observation and the changes in GR_{average} and *CS* indicate that small-chain SAS, i.e., more hydrophilic SAS, may enhance gas-to-particle mass transport, influencing the heterogeneous chemistry and promoting particle growth. Similar observations regarding the partitioning enhancement of hydrophobic or incompletely oxidized molecules by short-chain coated organics are reported in the literature [79]. Furthermore, field studies [38,81] have identified higher concentrations of organics, including partially oxidized and hydrophobic compounds, in fog water and aqueous aerosol particles than could be explained by Henry's law and the surrounding gas phase concentrations. Here, for the first time, we demonstrate that SAS can influence particle growth, potentially enhancing the transfer of incompletely oxidized compounds to the particle phase, which can, among others, explain the non-Henry's law behavior of different vapors. In conclusion, we believe that future research using the newly introduced electrochemical methodology will provide significant data on the importance of SAS and serve as a powerful tool for studying various atmospheric processes and related phenomena.

4. Conclusions

In this work, we developed a sensitive methodology for measuring changes in γ caused by SAS using an electrochemical approach. It is based on measuring changes in $I_{capacity}$ caused by the adsorption of SAS at the electrode surface that is proportional to the $d\gamma$. The electrochemical protocol was successfully combined with an environmentally friendly bismuth electrode as an excellent alternative to its mercury counterpart used in preliminary experiments. The new methodology effectively detects surface activity even at significantly lower concentrations of SAS in atmospheric particles compared to conventional tensiometric approaches. Introducing this methodology to measure changes in γ caused by SAS facilitates the investigation of various atmospheric processes, such as particle growth and CCN. The proposed electrochemical methodology study revealed that specific SAS could exhibit surface activity even at lower concentrations, a phenomenon not previously observed. Moreover, this approach offers the possibility of distinguishing the nature of different SAS. The results show that electrochemistry is a powerful tool for studying atmospheric processes by opening the door to a deeper understanding of the intricate surface chemistry that undoubtedly influences atmospheric particle growth. The applicability of the present electrochemical method in other fields warrants further research.

List of Abbreviations

AC	alternative current
μ	chemical potential
A	CPE coefficient representing pseudo admittance
Ag	silver
AgCl	silver chloride
BiBE	bismuth bulk electrode
CCN	cloud condensation nuclei
C_{diff}	differential capacitance
C_{dl}	double-layer capacitance
C_{eff}	effective double-layer capacitance
CPC	condensation particle counter
CPEs	constant phase elements
CS	condensation sink
CV	cyclic voltammogram
D	vapor diffusion coefficient
D_{AB}	binary diffusion coefficient of species A and B
dE	applied potential to the working electrode
$dI_{capacity}$	change in capacitive current
DMA	differential mobility analyzer
D_{max}	maximum size of critical clusters due to their growth during Δt
D_p	particle diameter
dp (10 nm)	measured particles of diameter upto 10 nm
D_{pg}	geometric mean diameter
$d\gamma$	change in surface tension
EIS	electrochemical impedance spectroscopy
FMG	Frumking-Melik-Gaikazyan
FRA	frequency response analyzer
$GR_{average}$	average growth rate
H_2SO_4	sulfuric acid
HTCO	high-temperature catalytic oxidation
$I_{capacity}$	capacitive current
j	complex number notation
J_{10}	apparent formation rate of new particle (dp (10 nm))
J_D	observed change in $N_{D,\ Dmax}$ during Δt
KCl	potassium chloride
M_{AB}	molecular weights of species A and B
MME	multi-mode mercury electrode
N	maximum number of possible individual modes in PNSD
NaCl	sodium chloride
$NaClO_4$	sodium perchlorate
$N_{D,\ Dmax}$	the total particle number concentration in the size range [D, D_{max}]
N_{dp}	continuous PNSD function
NPF	new particle formation
NSTD	normalized surface tension decrease
N_{tot}	total number concentration
OOM	oxidized organic molecules
P	pressure in Pa
p.z.c.	potential of zero charge
PM_1	particulate matter of aerodynamic diameter size $\leq$ 1μm
PNSD	particle number size distributions
R_{ad}	adsorption resistance
R_{el}	electrolyte resistance
SAS	surface-active substances
S-L	Szyszkowski-Langmuir
SMDE	static mercury drop electrode
SMPS	scanning mobility particle sizer
T	temperature in K
TOC	total organic carbon
TX-100	Triton-X-100
WSOC	water-soluble-organic carbon
Z_{Im}	imaginary part of the impedance
Z_w	Warburg coefficient
α	fractional exponent
$\beta_{m,dp}$	transition-regime correction factor
γ	surface tension

(*continued on next page*)

(*continued*)

Γ	surface excess concentration
ε	dielectric constant
σ_g^2	geometric variance
σ_M	surface charge on the electrode
Σ_v	summation of atomic diffusion volumes of each species
Ω	angular frequency

CRediT authorship contribution statement

Kristijan Vidović: Writing – review & editing, Writing – original draft, Visualization, Methodology, Investigation, Data curation, Conceptualization. **Samo B. Hočevar:** Writing – review & editing, Resources, Funding acquisition. **Kumar Sarang:** Writing – review & editing. **Ivan Konjević:** Writing – review & editing, Investigation. **Nikola Tasić:** Writing – review & editing. **Irena Ciglenečki:** Writing – review & editing, Funding acquisition.

Declaration of competing interest

The authors declare that they have no known competing financial interests or personal relationships that could have appeared to influence the work reported in this paper.

Acknowledgments

This research received funding from the Slovenian Research Agency (Program P1–0034) and the Croatian Science Foundation project IP-2018–01–1717 (MARRES).

Supplementary materials

Supplementary material associated with this article can be found, in the online version, at doi:10.1016/j.electacta.2025.145643.

Data availability

Data will be made available on request.

References

[1] V.F. McNeill, N. Sareen, A.N. Schwier, Surface-Active organics in atmospheric aerosols, in: V.F. McNeill, P.A. Ariya (Eds.), Atmospheric and Aerosol Chemistry, Springer Berlin Heidelberg, Berlin, Heidelberg, 2014, pp. 201–259.
[2] K.A. Wokosin, E.L. Schell, J.A. Faust, Emerging investigator series: surfactants, films, and coatings on atmospheric aerosol particles: a review, Environ. Sci.: Atmos. 2 (2022) 775–828.
[3] J.B. Gilman, H. Tervahattu, V. Vaida, Interfacial properties of mixed films of long-chain organics at the air–water interface, Atmos. Environ. 40 (2006) 6606–6614.
[4] M.C. Facchini, M. Mircea, S. Fuzzi, R.J. Charlson, Cloud albedo enhancement by surface-active organic solutes in growing droplets, Nature 401 (1999) 257–259.
[5] T.C. Burdette, A.A. Frossard, Characterization of seawater and aerosol particle surfactants using solid phase extraction and mass spectrometry, J. Environ. Sci. 108 (2021) 164–174.
[6] S.S. Petters, M.D. Petters, Surfactant effect on cloud condensation nuclei for two-component internally mixed aerosols, J. Geophys. Res.: Atmos. 121 (2016) 1878–1895.
[7] I. Ciglenečki, P. Orlović-Leko, K. Vidović, V. Tasić, The possible role of the surface active substances (SAS) in the airborne transmission of SARS-CoV-2, Environ. Res. 198 (2021) 111215.
[8] K. Vidović, S. Hočevar, I. Grgić, D. Metarapi, I. Dominović, B. Mifka, A. Gregorič, B. Alfoldy, I. Ciglenečki, Do bromine and surface-active substances influence the coastal atmospheric particle growth? Heliyon (2024) 10.
[9] B. Nozière, C. Baduel, J.-L. Jaffrezo, The dynamic surface tension of atmospheric aerosol surfactants reveals new aspects of cloud activation, Nat. Commun. 5 (2014) 3335.
[10] V. Gérard, B. Nozière, C. Baduel, L. Fine, A.A. Frossard, R.C. Cohen, Anionic, cationic, and nonionic surfactants in atmospheric aerosols from the Baltic coast at Askö, Sweden: implications for cloud droplet activation, Environ.Sci. Technol. 50 (2016) 2974–2982.
[11] H. Xi Yuan, M.J. Rosen, Dynamic surface tension of aqueous surfactant solutions: I. Basic paremeters, J. Colloid Interface Sci. 124 (1988) 652–659.
[12] D.M. Mott, M. Fukuyama, A. Hibara, Aerosol droplet surface measurement methods, Anal. Sci. 37 (2021) 61–68.
[13] J. Setschenow, Über die konstitution der salzlösungen auf grund ihres verhaltens zu kohlensäure, Zeitschrift für Physikalische Chemie 4U (1889) 117–125.
[14] K.J. Angle, C.M. Nowak, V.H. Grassian, Organic acid evaporation kinetics from aqueous aerosols: implications for aerosol buffering capacity in the atmosphere, Environ. Sci.: Atmos. 3 (2023) 316–327.
[15] B. Breyer, H.H. Bauer, Alternating Current Polarography and Tensammetry, Interscience Publishers, New York 16, N. Y., 1963, 605 Third Ave.
[16] W. Lorenz, F. Möckel, W. Müller, Zur adsorptionsisotherme organischer moleküle und molekülionen an quecksilberelektroden, I, Zeitschrift für Physikalische Chemie 25 (1960) 145–160.
[17] W. Lorenz, W. Müller, Zur adsorptionsisotherme organischer moleküle und molekülionen an quecksilberelektroden, II, Zeitschrift für Physikalische Chemie 25 (1960) 161–174.
[18] N. Batina, I. Ružić, B. Ćosović, An electrochemical study of strongly adsorbable surface-active substances: determinations of adsorption parameters for triton-X-100 at the mercury/sodium chloride interface, J. Electroanal. Chem. Interf. Electrochem. 190 (1985) 21–32.
[19] F.C. Anson, Patterns of ionic and molecular adsorption at electrodes, Acc. Chem. Res. 8 (1975) 400–407.
[20] B. Ćosović, V. Vojvodić, Voltammetric analysis of surface active substances in natural seawater, Electroanalysis 10 (1998) 429–434.
[21] V. Ɨutić, B. Ćosović, Z. Kozarac, Electrochemical determination of surface active substances in natural waters on the adsorption of petroleum fractions at mercury electrode/seawater interface, J. Electroanal. Chem. Interf. Electrochem. 78 (1977) 113–121.
[22] S. Trasatti, Acquisition and analysis of fundamental parameters in the adsorption of organic substances at electrodes, J. Electroanal. Chem. Interf. Electrochem. 53 (1974) 335–363.
[23] S. Trasatti, Adsorption of organic substances at electrodes: recent advances, Electrochim. Acta 37 (1992) 2137–2144.
[24] B. Cosović, V. Vojvodić, The application of AC polarography to the determination of surface-active substances in seawater, Limnol. Oceanogr. 27 (1982) 361–369.
[25] B.B. Damaskin, Adsorption of organic compounds [at the mercury electrode – solution interface], Russ. Chem. Rev. 34 (1965) 752.
[26] M. Ochs, Coordinative and Hydrophobic Interaction of Humic Substances With Aquatic Surfaces, ETH Zurich, 1991.
[27] A.J. Bard, L.R. Faulkner, H.S. White, Electrochemical Methods: fundamentals and Applications, 3rd ed., John Wiley & Sons 2022.
[28] A. Bain, Recent advances in experimental techniques for investigating aerosol surface tension, Aerosol Sci. Technol. 58 (2024) 1213–1236.
[29] H. Nakadomari, D.M. Mohilner, P.R. Mohilner, Electrosorption of 2-butanol at the mercury-solution interface. 1. Thermodynamic treatment, J. Phys. Chem. 80 (1976) 1761–1772.
[30] J. Richer, J. Lipkowski, Measurement of physical adsorption of neutral organic species at solid electrodes, J. Electrochem. Soc. 133 (1986) 121.
[31] V.S. Markin, A.G. Volkov, Electrocapillary phenomena at the interface between two immiscible liquids, Prog. Surf. Sci. 30 (1989) 233–356.
[32] L. Meites, Studies in the theory of the polarographic diffusion current. V. Effects of certain variables on m and the residual current, J. Am. Chem. Soc. 73 (1951) 2035–2037.
[33] D. Krznarić, T. Goričnik, M. Vuković, D. Čukman, Humic acid adsorption on the Au (111) and Au polycrystalline electrode surface, Electroanalysis 13 (2001) 109–116.
[34] M. Gerlache, J.M. Kauffmann, G. Quarin, J.C. Vire, G.A. Bryant, J.M. Talbot, Electrochemical analysis of surfactants: an overview, Talanta 43 (1996) 507–519.
[35] L.-H. Shao, J. Biener, D. Kramer, R.N. Viswanath, T.F. Baumann, A.V. Hamza, J. Weissmüller, Electrocapillary maximum and potential of zero charge of carbon aerogel, Phys. Chem. Chem. Phys. 12 (2010) 7580–7587.
[36] J.O.M. Bockris, M.A.V. Devanathan, K. Müller, On the structure of charged interfaces, in: J.A. Friend, F. Gutmann (Eds.), Electrochemistry, Pergamon, 1965, pp. 832–863.
[37] R.G. Barradas, J.M. Sedlak, Some observations on recent theories of adsorption of organic compounds in the double layer, Electrochim. Acta 17 (1972) 1901–1905.
[38] D.E. Glotfelty, M.S. Majewski, J.N. Seiber, Distribution of several organophosphorus insecticides and their oxygen analogs in a foggy atmosphere, Environ.Sci. Technol. 24 (1990) 353–357.
[39] J. Ehrlich, T. Ehrlich, A. Jänes, E. Lust, The zero charge potential shift upon adsorption of various organic compounds at bismuth|solution interface, Electrochim. Acta 45 (1999) 935–943.
[40] H.R. Zebardast, S. Rogak, E. Asselin, Potential of zero charge of glassy carbon at elevated temperatures, J. Electroanal. Chem. 724 (2014) 36–42.
[41] B. Ter-Ovanessian, C. Alemany-Dumont, B. Normand, Single frequency electrochemical impedance investigation of zero charge potential for different surface states of Cu–Ni alloys, J. Appl. Electrochem. 44 (2014) 399–410.
[42] A. Anastopoulos, A. Papoutsis, A. Papaderakis, Differential capacitance and electrochemical impedance study of surfactant adsorption on polycrystalline Ni electrode, J. Solid State Chem. 19 (2015) 2369–2377.
[43] D. Krznarić, T. Goričnik, B. Ćosović, Electrochemical determination of organic surface active substances in model and natural sea water with Au (lll) monocrystal electrode, Croatica Chemica Acta 73 (2000) 247–261.
[44] R.D. Armstrong, W.P. Race, H.R. Thirsk, The kinetics of adsorption of neutral organic compounds at a mercury electrode, J. Electroanal. Chem. Interf. Electrochem. 16 (1968) 517–529.

[45] S. Trasatti, E. Lust, The potential of zero charge, in: R.E. White, J.O.M. Bockris, B. E. Conway (Eds.), Modern Aspects of Electrochemistry, Springer New York, NY, 1999, pp. 1–215.
[46] A.W. Adamson, A.P. Gast, Physical Chemistry of Surfaces, 6th ed.6th ed., John Wiley & Sons Inc, 1997.
[47] S. Decesari, M.C. Facchini, M. Mircea, F. Cavalli, S. Fuzzi, Solubility properties of surfactants in atmospheric aerosol and cloud/fog water samples, J. Geophys. Res.: Atmos. 108 (2003) 4685.
[48] G. Kiss, E. Tombácz, H.-C. Hansson, Surface tension effects of humic-like substances in the aqueous extract of tropospheric fine aerosol, J Atmos Chem 50 (2005) 279–294.
[49] I. Taraniuk, E.R. Graber, A. Kostinski, Y. Rudich, Surfactant properties of atmospheric and model humic-like substances (HULIS), Geophys. Res. Lett. 34 (2007).
[50] F. Scholz, Voltammetric techniques of analysis: the essentials, ChemTexts 1 (2015) 17.
[51] I. Ciglenečki, P. Orlović-Leko, K. Vidović, N. Simonović, M. Marguš, J. Dautović, S. Mateša, I. Galić, The possibilities of voltammetry in the study reactivity of dissolved organic carbon (DOC) in natural waters, J. Solid State Electrochem. 27 (2023) 1781–1793.
[52] R. Tuckermann, Surface tension of aqueous solutions of water-soluble organic and inorganic compounds, Atmos. Environ. 41 (2007) 6265–6275.
[53] A.-P. Hyvärinen, H. Lihavainen, A. Gaman, L. Vairila, H. Ojala, M. Kulmala, Y. Viisanen, Surface tensions and densities of oxalic, malonic, succinic, maleic, malic, and cis-pinonic acids, J. Chem. Eng. Data 51 (2006) 255–260.
[54] Z. Varga, G. Kiss, H.C. Hansson, Modelling the cloud condensation nucleus activity of organic acids on the basis of surface tension and osmolality measurements, Atmos. Chem. Phys. 7 (2007) 4601–4611.
[55] F. Cavalli, M.C. Facchini, S. Decesari, M. Mircea, L. Emblico, S. Fuzzi, D. Ceburnis, Y.J. Yoon, C.D. O'Dowd, J.-P. Putaud, A. Dell'Acqua, Advances in characterization of size-resolved organic matter in marine aerosol over the North Atlantic, J. Geophys. Res.: Atmos. 109 (2004).
[56] I. Švancara, C. Prior, S.B. Hočevar, J. Wang, A decade with bismuth-based electrodes in electroanalysis, Electroanalysis 22 (2010) 1405–1420.
[57] S.B. Hočevar, B. Ogorevc, J. Wang, B. Pihlar, A study on operational parameters for advanced use of bismuth film electrode in anodic stripping voltammetry, Electroanalysis 14 (2002) 1707–1712.
[58] E.A. Hutton, S.B. Hočevar, B. Ogorevc, Ex situ preparation of bismuth film microelectrode for use in electrochemical stripping microanalysis, Anal. Chim. Acta 537 (2005) 285–292.
[59] J. Wang, J. Lu, S.B. Hocevar, B. Ogorevc, Bismuth-Coated screen-printed electrodes for stripping voltammetric measurements of trace lead, Electroanalysis 13 (2001) 13–16.
[60] R. Pauliukaitė, S.B. Hočevar, B. Ogorevc, J. Wang, Characterization and applications of a bismuth bulk electrode, Electroanalysis 16 (2004) 719–723.
[61] A. Lasia, Definition of Impedance and Impedance of Electrical Circuits. Electrochemical Impedance Spectroscopy and Its Applications, Springer New York, NY, 2014, pp. 7–66.
[62] M.E. Orazem, B. Tribollet, Electrochemical Impedance Spectroscopy, John Wiley & Sons, Inc, 2008.
[63] A. Jänes, K. Lust, E. Lust, Adsorption kinetics of D-ribose on the bismuth(001) plane, J. Electroanal. Chem. 548 (2003) 27–39.
[64] E. Lust, A. Jänes, P. Miidla, K. Lust, Adsorption of pyridine on the (111), (001) and (001) faces of bismuth, J. Electroanal. Chem. 425 (1997) 25–37.
[65] V.D. Jović, B.M. Jović, EIS and differential capacitance measurements onto single crystal faces in different solutions: part I: ag(111) in 0.01 M NaCl, J. Electroanal. Chem. 541 (2003) 1–11.
[66] V. Jović, Differential capacity of bromide anions adsorption onto Ag(100) in the absence, and onto Ag(poly) in the presence of $NaClO_4$, Chem. Biochem. Eng. Q. 23 (2009) 11–22.
[67] M. Sluyters-Rehbach, J.H. Sluyters, Sine Wave Methods in the Study of Electrode Processes, 1970.
[68] G. Nurk, H. Kasuk, K. Lust, A. Jänes, E. Lust, Adsorption kinetics of dodecyl sulfate anions on the bismuth(011¯) plane, J. Electroanal. Chem. 553 (2003) 1–19.
[69] B.-Y. Chang, Conversion of a constant phase element to an equivalent capacitor, J. Electrochem. Sci. Technol. 11 (2020) 318–321.
[70] G.J. Brug, A.L.G. van den Eeden, S.-R. Margaretha, J.H. Sluyters, The analysis of electrode impedances complicated by the presence of a constant phase element, J. Electroanal. Chem. Interf. Electrochem. 176 (1984) 275–295.
[71] C. Hsu, F. Mansfeld, Concerning the conversion of the constant phase element parameter Y_0 into a capacitance, Corrosion (2001) 57.
[72] M.N. Kakaei, J. Neshati, A.R. Rezaierod, On the extraction of the effective capacitance from constant phase element parameters, Prot. Met. Phys. Chem. Surf. 54 (2018) 548–556.
[73] K. Vidović, A. Kroflič, P. Jovanovič, M. Šala, I. Grgić, Electrochemistry as a tool for studies of complex reaction mechanisms: the case of the atmospheric aqueous-phase aging of catechols, Environ. Sci. Technol. 53 (2019) 11195–11203.
[74] A. Kroflič, S. Frka, M. Simmel, H. Wex, I. Grgić, Size-Resolved surface-active substances of atmospheric aerosol: reconsideration of the impact on cloud droplet formation, Environ. Sci. Technol. 52 (2018) 9179–9187.
[75] M. Dal Maso, M. Kulmala, I. Riipinen, R. Wagner, T. Hussein, P.P. Aalto, K. E. Lehtinen, Formation and growth of fresh atmospheric aerosols: eight years of aerosol size distribution data from SMEAR II, Hyytiälä, Finland, Boreal Environ. Res. 10 (2005) 323–336.
[76] S. Buenrostro Mazon, I. Riipinen, D.M. Schultz, M. Valtanen, M. Dal Maso, L. Sogacheva, H. Junninen, T. Nieminen, V.M. Kerminen, M. Kulmala, Classifying previously undefined days from eleven years of aerosol-particle-size distribution data from the SMEAR II station, Hyytiälä, Finland, Atmos. Chem. Phys. 9 (2009) 667–676.
[77] Z. Németh, B. Rosati, N. Zíková, I. Salma, L. Bozó, C. Dameto de España, J. Schwarz, V. Ždímal, A. Wonaschütz, Comparison of atmospheric new particle formation events in three central European cities, Atmos. Environ. 178 (2018) 191–197.
[78] S. Tuovinen, J. Kontkanen, R. Cai, M. Kulmala, Condensation sink of atmospheric vapors: the effect of vapor properties and the resulting uncertainties, Environ. Sci.: Atmos. 1 (2021) 543–557.
[79] B.T. Mmereki, D.J. Donaldson, Laser induced fluorescence of pyrene at an organic coated air–water interface, Phys. Chem. Chem. Phys. 4 (2002) 4186–4191.
[80] M.S. Bakshi, How surfactants control crystal growth of nanomaterials, Cryst. Growth Des. 16 (2016) 1104–1133.
[81] C.J. Schomburg, D.E. Glotfelty, J.N. Seiber, Pesticide occurrence and distribution in fog collected near Monterey, California, Environ. Sci. Technol. 25 (1991) 155–160.